J Mater Sci (2010) 45:5698–5703
DOI 10.1007/s10853-010-4639-5

Photocatalyst TiO_2–Co: the effect of doping depth profile on methylene blue degradation

Hudson W. P. Carvalho · Ana P. L. Batista · Roberto Bertholdo · Celso V. Santilli · Sandra H. Pulcinelli · Teodorico C. Ramalho

Received: 8 October 2009 / Accepted: 21 May 2010 / Published online: 16 June 2010

Abstract In this work, we study the effect of doping depth profile on the photocatalytic and surface properties of TiO_2 films. Two thin film layers of TiO_2 (200 nm) and Co (5 nm), respectively, were deposited by physical evaporation on glass substrate. These films were annealed for 1 s at 100 and 400 °C and the Co layer was removed by chemical etching. Atomic force microscopy (AFM) phase images showed changes in the surface in function of thermal treatment. The grazing-incidence X-ray fluorescence (GIXRF) measurements indicated that the thermal treatment caused migration of Co atoms to below the surface, the depths found were between 19 and 29 nm. The contact angle showed distinct values in function of the doped profile or Co surface concentration. The UV–vis spectra presented a red shift with the increasing of thermal treatment. Photocatalytical assays were performed by methylene blue discoloration and the higher activity was found for TiO_2–Co treated at 400 °C, the ESI-MS showed the fragments formed during the methylene blue decomposition.

H. W. P. Carvalho (✉) · R. Bertholdo · C. V. Santilli · S. H. Pulcinelli
Departamento de Físico-Química, Instituto de Química, Universidade Estadual Paulista, CP 355, Araraquara, SP 14800-900, Brazil
e-mail: hudsonwpc@yahoo.com.br

A. P. L. Batista
Departamento de Química Fundamental, Instituto de Química, Universidade de São Paulo, CEP 05508-000 São Paulo, SP, Brazil

T. C. Ramalho
Departamento de Química, Universidade Federal de Lavras, CP 3037, Lavras, MG 37200-000, Brazil

Introduction

There are many treatment techniques for wastewater remediation, among them, we can highlight advanced oxidative processes that produce hydroxyl radicals ($OH^{\bullet}$) [4]. One way to produce $OH^{\bullet}$ radicals consists of irradiation by UV light on semiconductors. When irradiated with enough energy these materials can generate electron–hole pairs, which may react with the surface hydroxyl groups, OH, oxygen molecules and O_2 absorbed on the surface of the catalyst, thus yielding hydroxyl radical and the super oxide radical ion, respectively. Such species have high activity and can oxidize organic compounds. Another pathway consists of a direct reaction between holes and organic pollutant, depending on the properties of both the substance and the photocatalyst. In this case, the radical derived from the pollutant molecule can react both with $OH^{\bullet}$ radicals and dissolved oxygen [17].

The TiO_2 is largely utilized as a photocatalyst, and several works have employed doping with Co atoms to improve the photocatalityc properties [11, 13]. The TiO_2 have a band gap around 3.20 eV, that corresponds to 388 nm, and many efforts have been made to decrease the band gap energy. The doping process with transition metals seems to be efficient in reducing the energy necessary for these transitions [1].

Another approach consists of the creation of other reaction mechanism on TiO_2 surfaces; the doping process of semiconductors with transitions metals could lead to Fenton-like mechanisms in systems containing H_2O_2. Then, the doping process could cause a red shift on TiO_2 and supply other reactive sites for H_2O_2 decomposition [12].

Cobalt is a relatively abundant metal and is frequently found with other ones such as iron and nickel, thus it could be an attractive dopant [7, 10]. Therefore, in this work, we

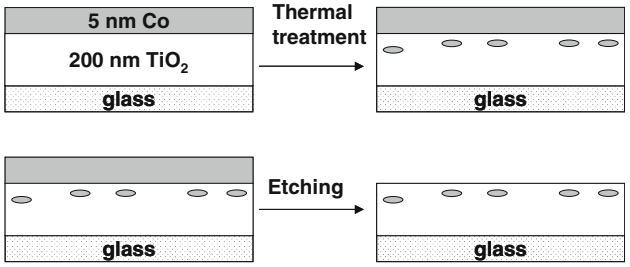

Fig. 1 Sample preparation

aim to understand the effects of the depth profile and Co concentration on the surface properties of TiO_2.

Experiments

Sample preparation

In the first step of the sample preparation process, shown in Fig. 1, 200 nm thick TiO_2 films were deposited on glass substrates (2 × 2 cm, borosilicate, Corning 7070) by DC sputtering (Balzers BA510). The main chamber base pressure was kept at 2×10^{-7} mbar, Ti (99.999%) was employed as target, and the reactive gas mixture consisted of O_2 (99.99%) and Ar (99.99%). On the top of the TiO_2 film, a 5 nm thick Co layer was deposited by DC sputtering using a Co target (99.999%) and Ar (99.99%) working gas. In both depositions, the adjusted power was 800 W.

The photocatalyst materials were obtained by thermally induced diffusion of Co atoms into the TiO_2 films. For this purpose, the samples were submitted to thermal treatment for 1 s at 100 and 400 °C in argon atmosphere, using a rapid thermal processing system (RTA AG Heat Pulse 410). A set of non-annealed samples were used as reference. After annealing, the Co films were removed by chemical etching (10 mL hydrogen peroxide (30% v/v), 50 mL of sulfuric acid, and 440 mL of water; corrosion rate of 1 μm min^{-1}), leaving only a Co-doped TiO_2 surface region. The samples were named following the thermal treatment: TiO_2–Co-WT, TiO_2–Co-100, and TiO_2–Co-400.

Characterization

The surface morphology was investigated by atomic force microscopy (AFM). The images were collected under ambient conditions using an Agilent 5500 microscope operating in acoustic AC mode. Silicon tips (NanoWorld) with spring constants of 42 N m^{-1} and 320 kHz resonance frequency were used.

Contact angle measurements with the sessile drop method were recorded and analyzed using an OCA-20 Contact Angle System (DataPhysics Instruments). Testing liquids with different polarity and surface tension were used: glycerol ($\sigma_{L,V}$ = 65.20 mN/m), NaCl 3.5% solution ($\sigma_{L,V}$ = 73.76 mN/m), and ultra pure water ($\sigma_{L,V}$ = 72.30 mN/m, MilliQ, Millipore). A drop of liquid (10 μL) was placed, at 1 μL/s velocity, on the thin films, and the contact angle was measured. Measurements were performed at three different points on each film and the mean value was calculated. The accuracy of the contact angles was estimated as ±1% [16]. The UV–vis spectra were recorded by using a Cary 500 Scan spectrophotometer. The absorption (a/S) data were calculated from the reflectivity using the Kubelka–Munk transformation. Usually, optical gaps are determined after a Kubelka–Munk transformation of the reflectivity spectrum as the intersection point between the energy axis and the line extrapolated from the linear portion of the absorption threshold.

The grazing-incidence X-ray fluorescence (GIXRF) measurements were performed at the XRF beamline of the Brazilian Synchrotron Light Laboratory (LNLS). The synchrotron radiation (SR), produced by the DO9B (15°) bending magnet of the storage ring, was monochromatized by double crystal "channel-cut" monochromator equipped with a Si (111) crystal. The beam intensity was monitored with an ionization chamber. The detection system consists of a Ultra-LEGe solid state detector to collect the X-ray fluorescence and scattered radiation coming from the sample. Samples were placed on a special holder attached to a high-resolution goniometer (0.001° angular resolution). The monochromatic beam was collimated with orthogonal slits to 4 mm × 0.2 mm in the horizontal and vertical direction, respectively. A 8.5 keV beam energy was selected, which is slightly above the Co Kα absorption edge.

Photoactivity measurements

The measurements were carried out with 1 mL of hydrogen peroxide solution, H_2O_2 (30% v/v) (Merck), and 50 mL (mg L^{-1}) of methylene blue (Petroquímios), at pH 6.5. The films were put on a reactor and the degradation of methylene blue solution was evaluated under UV light, provided by a high-pressure mercury lamp (HPK 125 W, Philips). All reactions were carried out at 25 °C. Liquid aliquots were removed at intervals of 10, 25, and 45 min; dye photodegradation was monitored by measuring the absorbance at 665 nm with a ShimadzuUVPC 1600 spectrophotometer (UV/vis).

ESI-MS study

To identify the intermediates formed during the methylene blue decomposition, mass spectrometry with electron spray ionization interface at positive mode of an Agilent MS ion-trap mass spectrometer was used. After 10 min of reaction

time, one aliquot was collected and injected into the ESI source with a syringe pump at a flow rate of 5 mL min^{-1}. The spectra were obtained as an average of 50 scans of 0.2 s. The ESI conditions were as follows: heated capillary temperature of 325 °C; sheath gas (N_2) at a flow rate of (6 L min^{-1}); spray voltage of 4 kV; capillary tension of 25 V; tube lens off set tension of 25 V.

Results and discussion

Figure 2 shows the AFM phase images of the TiO_2–Co photocatalysts. Phase imaging is useful to differentiate the component phases of materials through sensing local variations in hardness, viscoeleasticity, or adhesion [3]. Figure 2 clearly shows the light spot diminution with the thermal treatment evolution. These spots can be attributed to Co particles that are spread out to the TiO_2 layer under high temperatures.

The contact angle is a surface property consequent from intermolecular interactions. Contact angle measurements are related to surface tensions or energies via Young's equation: $\gamma_{sv} = \gamma_{sl} + \gamma_{lv} \cos\theta$, where θ is the measured contact angle and γ is the surface energy of the solid–vapor (sv), solid–liquid (sl), and liquid–vapor (lv) interface. From contact angle measurements, we have extracted the solid surface energy employing the Owens–Wendt–Rabel–Kaelble method [8]. It is an important property influencing the wettability, since that photocatalytic reaction occurs at an interface between solution and photocatalyst surface. Surface energy depends on the chemical structure of the solid; the wettability also depends on the surface morphology and on the contact liquid [8].

Table 1 shows the contact angle of samples. Apparently TiO_2–Co-100 presents more hydrophilic features in NaCl 3.5% than water. When compared TiO_2-100 and TiO_2-400, the first one has shown more affinity by the polar solvents, but these differences were close of experimental error. In glycerol medium the TiO_2–Co-WT was the more wettable surface. The interesting fact is that the decrease at the contact angle is not linearly dependent on the Co concentration, and seemingly the thermal treatment could also played a role on the wettability. A similar behavior was described for TiO_2–Mn films, where doping reduces and increases the contact angle, depending on the dopant concentration increase [15]. The influence of Co could be related to changes in the cation equilibrium at the surface, the presence of Co metal dopant can change the relation of Ti^{4+} and Ti^{3+} at the surface, Ti^{4+}–$O^{2-} \leftrightarrow Ti^{3+}$–$O^{-}$ [1]. When Ti^{3+} is formed the excess oxygen can be ejected from the surface and the oxygen vacancies filled by water molecules forming the OH groups, therefore increasing the wettability [15].

Table 1 Contact angle with different solvents and surface free energy

Thin film	Surface energy (mN/m)	θ (°)		
		Water	NaCl 3.5%	Glycerol
TiO_2–Co-WT	62	33	39	34
TiO_2–Co-100	86	32	25	45
TiO_2–Co-400	68	36	35	39

In a GIXRF experiment, a high-collimated monochromatic beam excites the sample at shallow angles, usually less than 1°. The angular dependence of the fluorescence signal was measured below and above the critical angle for total external reflection of the incident X-rays, covering an angular range from 0° to 0.6°.

Figure 3 shows the experimental and calculated GIXRF data, it was possible to find good concordance among the data. The fitting data TiO_2–Co-WT (Fig. 3a) showed Co up to 19–20 nm below the TiO_2 surface. It is possible for metal self-diffusion to occur at room temperature, or during the sputtering deposition (around 70 °C). Zhou and Chen studied the diffusion of Cu in the TiO_2. In this work the authors monitored the diffusion of Cu in function of time at room temperature and reported a depth up to 4.8 Å after 30 min [18]. The GIXRF measured in this work was performed 20 days after deposition of Cu thin film, so it is possible that the Co atoms were diffused to this depth. Still in the matter of Co diffusion, Co ion implantation (25 keV) in the silicon substrate showed presence of Co up to 60 nm.

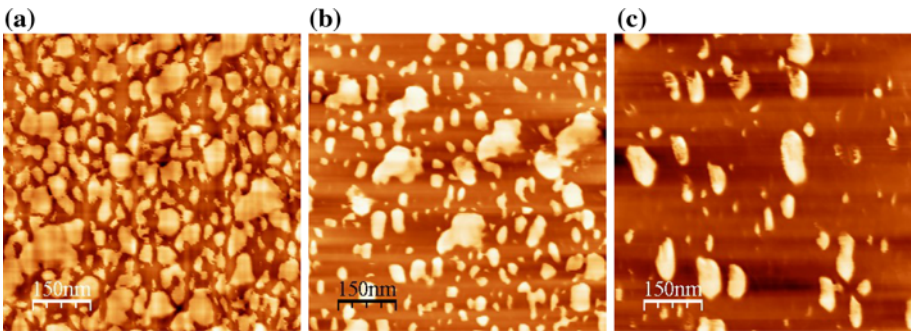

Fig. 2 AFM phase images: **a** TiO_2–Co-WT, **b** TiO_2–Co-100, and **c** TiO_2–Co-400

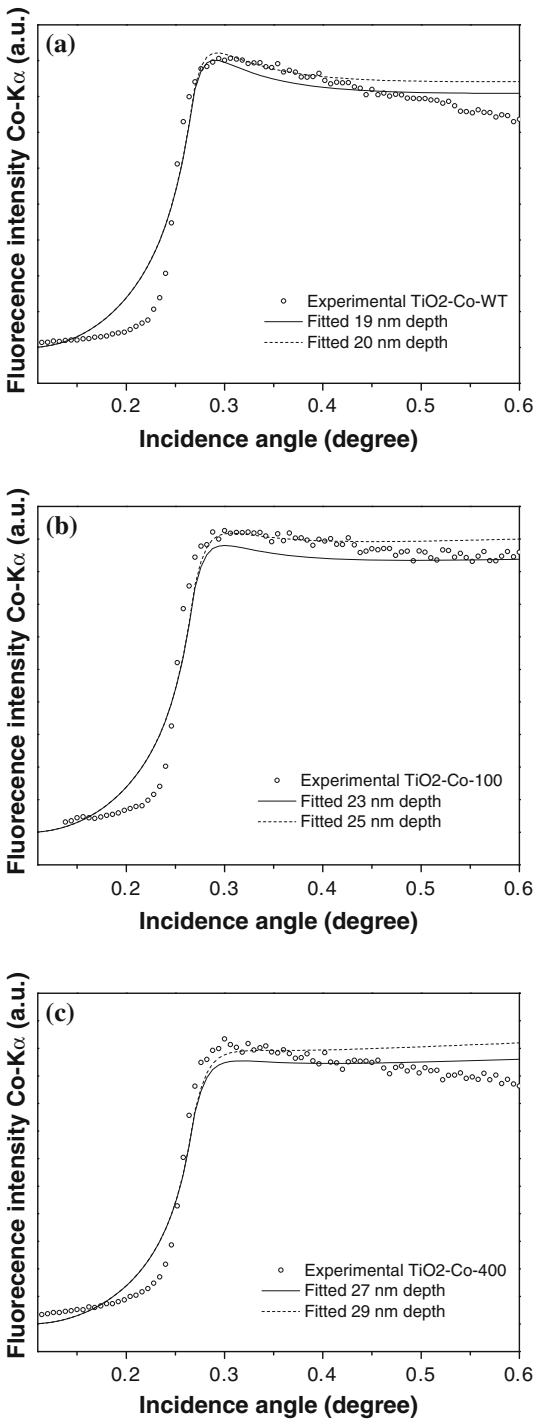

Fig. 3 Experimental and fitted GIXRF curves appointing the depth of Co bellow the TiO_2 surface: **a** TiO_2–Co-WT, **b** TiO_2–Co-100, and **c** TiO_2–Co-400

In fact this study compares the GIXRF, RBS, and ion sputtering to determine the depth profile concentration, and the GIXRF showed good concordance with other techniques [9].

In the TiO_2–Co-100, Co atoms were found around 23–25 nm (Fig. 3b). This result is coherent with the thermal treatment and for TiO_2–Co-400 (Fig. 3c), Co atoms were found at a 27–29 nm depth. As expected, the depth penetration increases with temperature of the thermal treatment, because of the diffusion. So far the concentration of Co has not been determined, only the maximum depth.

The diffusion processes are dependent on the temperature and are the activated processes. The depth profiles of ion implantation or diffusion present a concentration gradient, which decreases in function of depth. Other measurements by XPS performed by our research group have demonstrated that in the first 3 nm the doping concentration is higher for films treated at higher temperatures than at lower temperatures.

One interesting point is that the variation of the diffusion depth found in this work is not so contrasting to that observed in the diffusion of Cu and Au, in silicon, for example. In the other study, the non-thermally treated material, presented metal doping around 4 nm below the surface, while for the thermally treated metal doping can be found up to 45 nm. It seems that the temperature range employed is not enough to cause meaningful differences [12].

UV light can excites the electrons from the valence to the conduction bands creating electron/hole pairs. The excited electrons are high reductive species, while the holes are oxidants. In this way, the doping process can influences at least two points: the energy necessary for transitions to take place, and the life time of the electron–hole pair. The UV–vis spectra (Fig. 4) showed a slight bathochromic shift for the TiO_2–Co-100 sample. The optical band gap found from extrapolation of the UV-vis spectra of TiO_2 anatase, TiO_2–Co-WT, TiO_2–Co-100, TiO_2–Co-400, were 3.20, 3.20, 3.13 and 3.18 eV, respectively. Therefore, although small, we can infer that the doping process had some influence on decreasing the band gap. In the literature, other transition metals have been employed to promote red shifts on TiO_2. Apparently, the

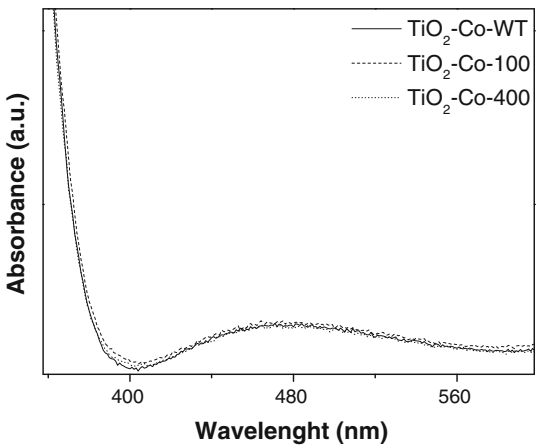

Fig. 4 UV–vis spectra obtained in reflectance mode and converted to absorbance with the Kulbelka–Munk function

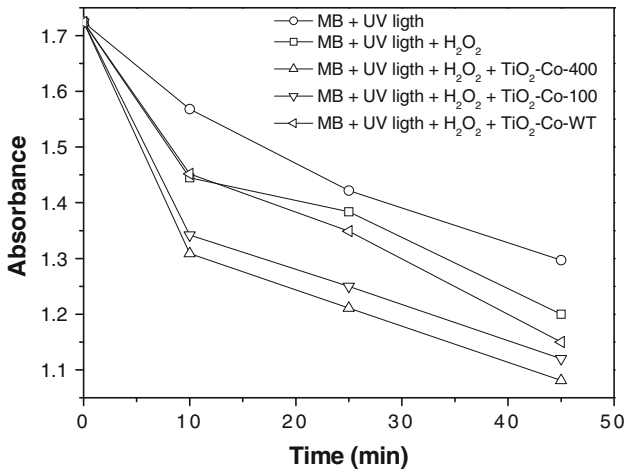

Fig. 5 Methylene blue discoloration by photocatalyst thin films

efficiency in reaching this objective has the following sequence V > Cr > Mn > Fe > Ni [1].

Other works in the literature have demonstrated more significant shifts, but in samples obtained by sol–gel methods and with higher amounts of Co still, in our study, the main objective is the relation between depth profile and its effect on the surface activity for photocatalytical employment.

The photocatalytic activity was evaluated through the methylene blue degradation. Figure 5 shows the absorbance in function of time. As the essays took place under UV light methylene blue is subjected to photolysis. The addition of H_2O_2 to the medium accelerated the methylene blue decomposition, H_2O_2 is decomposed forming $2OH^{\bullet}$, and it is well known that this radical is a strong oxidant.

The TiO_2–Co-400 had the major activity, and all TiO_2–Co had a meaningful difference when compared to the methylene blue/H_2O_2 leading to the conclusion that the photocatalyst surface reacts with the H_2O_2 or/and the methylene blue. The TiO_2–Co-400 demonstrated the highest photoactivity, on a first analysis it could be related to the concentration of Co ions at the surface. We suppose there are at least two active regions at the surface, the TiO_2 and Co species sites. At first, on TiO_2 the reaction among the electron/hole pair and H_2O_2, H_2O, O_2, or methylene blue leading to oxide or reduced species can occur. These mechanisms are well explored in several works [14]. Another hypothesis consists of the reaction between Co^0, Co^{2+}, or Co^{3+} with the H_2O_2 resulting in a kind of Fenton-like mechanism, according to the following equation:

$$Co^0,\ Co^{1+},\ \text{or}\ Co^{2+} + H_2O_2 \rightarrow Co^{1+},\ Cu^{2+},\ \text{or}\ Co^{3+} + OH^- + OH^{\bullet}$$

$$TiO_2 + h\nu \rightarrow h^+/e^-$$

$$Co^{1+},\ Co^{2+},\ \text{or}\ Co^{3+} + e^- \rightarrow Co^0,\ Co^{1+},\ \text{or}\ Co^{2+}.$$

This suggestion is consistent with recent studies, where H_2O_2 has been catalytically decomposed by surface materials [6].

The formation of $OH^{\bullet}$ radical and subsequent reaction hypothesis is reinforced by ESI-MS spectra (Fig. 6). Figure 6a shows the mass spectra of pure methylene blue before reaction, the signal at $m/z = 284$ corresponds to methylene blue molecule. However, in Fig. 6b, we can see the signal of the methylene blue molecule $m/z = 284$, and other signals that correspond to fragments, which arose during the decomposition of the methylene blue. The signal at $m/z = 284$ could be seen because the spectrum was taken 10 min after the decomposition start, then at that moment both structures were present in solution.

Previous studies developed by our research group, have shown that the signals at $m/z = 300$ and $m/z = 316$ can be attributed to successive hydroxylation of colorant structure due to $OH^{\bullet}$ attack [2]. The other signals correspond to fragmentation of the molecular structure; some studies on

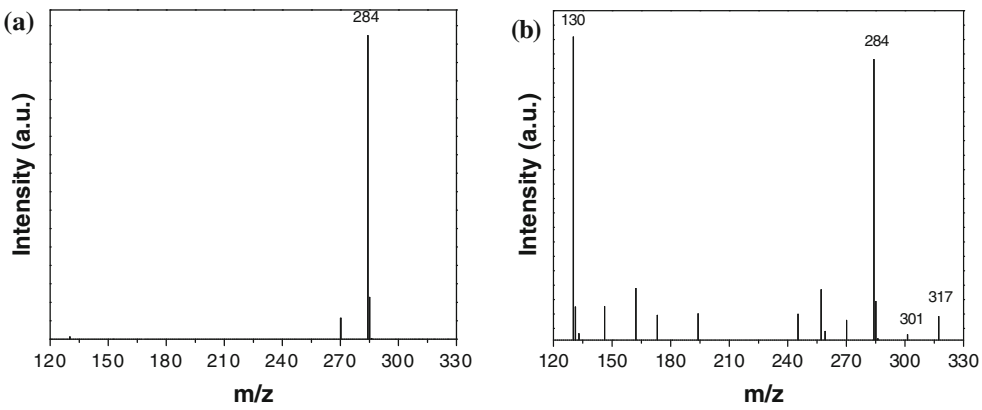

Fig. 6 ESI-MS spectra: **a** standard methylene blue, **b** obtained 10 min after onset of the discoloration reaction

the decomposition of methylene blue by hydroxyl radicals have shown that the colorant is completely mineralized [5].

Conclusions

Surface properties and photocatalytic activity of cobalt doped TiO_2 films were investigated for different doping depth of Co. AFM phase images have shown a high contrast among the surface, the treatment changes the morphology. We believe that these changes are different TiO_2 phase, and not Co islands. The GIXRF measurements indicated that the thermal treatment has little influence on Co migration depth. This could be related to activation energy of diffusion, Co depth below the TiO_2 surface varies between 19 and 29 nm. The doping process caused only few changes at the UV–vis spectra. Although the AFM showed different morphology, the contact angle measurements have shown a small difference among the samples. Photocatalytical tests performed by methylene blue discoloration have shown differences among the three samples; the sample treated at 400 °C has shown the higher activity. These differences can be attributed just to Co concentration on TiO_2 surface, due the Fenton-like mechanism hypothesis Co atoms can react to H_2O_2.

Acknowledgements We are grateful to FAPEMIG, FAPESP, CAPES and CNPq for funding part of this work. This work has been supported by the Brazilian Synchrotron Light Source (LNLS) under proposal D09B-XRF 7673/08.

References

1. Anpo M, Takeuchi M (2003) J Catal 216:505
2. Batista APL, Carvalho HWP, Luz GHP, Martins PFQ, Gonçalves M, Oliveira LCA (2008) Environ Chem Lett. doi:10.1007/s10311-008-0192-8
3. Behrend OP, Odoni L, Loubet JL, Burnham NA (1999) App Phys Lett 75:2551
4. Brown MA, Devito SC (1993) Crit Rev Environ Sci Technol 23:249
5. Esteves AO, Oliveira LCA, Ramalho TC, Gonçalves M, Anastacio AS, Carvalho HWP (2008) Catal Commun 10:330
6. Guimaraes IR, Giroto A, Oliveira LCA, Guerreiro MC, Lima DQ, Fabris JD (2009) Appl Catal B 91:581
7. Iawasaki MI, Hara M, Kawada H, Tada H, Ito S (2000) J Colloid Interface Sci 224:202
8. Janssen D, De Palma R, Verlaak S, Heremans P, Dehaen W (2006) Thin Solid Films 515:1433
9. Krzyzanowska H, von Bohlen A, Klockenkamper R (2003) Spectrochim Acta B 58:2059
10. Li J, Liu S, He Y, Wang J (2008) Micropor Mesopor Mater 115:416
11. Merabet S, Robert D, Weber JV, Bouhelassa M, Benkhanouche S (2009) Environ Chem Lett 7:45
12. Ramalho TC, Carvalho HWP, Batista APL, Perez CA, Gobbi AL (2009) J Mater Sci 44:1029. doi:10.1007/s10853-008-3206-9
13. Rehman S, Ullah R, Butt AM, Gohar ND (2009) J Hazard Mater 170:560
14. Robert D, Dongui B, Weber JV (2003) Photochem Photobiol A 156:195
15. Sharma SD, Saini KK, Kant C, Sharma CP, Jain SC (2008) Appl Catal B 84:233
16. Watanabe T, Fukayama S, Myauachi M, Fujishima A, Hashimoto K (2000) J Sol-Gel Sci Technol 19:71
17. Zhang L, Li J, Chen Z, Tang Y, Yu Y (2006) Appl Catal A 299:292
18. Zhou J, Chen DA (2003) Surf Sci 527:183